KEYNOTE

Generation and identification of 1,4-perinaphthadiyl radical cation—first observation of the electronic absorption spectrum of an ionized diradical

Zhendong Zhu,†,[a] Thomas Bally,*,[a] Jakob Wirz,[b] and Markus Fülscher[c]

[a] *Institute of Physical Chemistry, University of Fribourg, Pérolles, CH-1700 Fribourg, Switzerland*
[b] *Institute of Physical Chemistry, University of Basel, Klingelbergstrasse 80, CH-4056 Basel, Switzerland*
[c] *Department of Theoretical Chemistry, Chemical Centre, P.O.B. 124, S-22100 Lund, Sweden*

γ-Irradiation of 6b,7,8,8a-tetrahydrocyclobut[*a*]acenaphthylene (CAN) in haloalkane glasses at 77 K yields a persistent radical cation, CAN$^{\bullet+}$, whose electronic absorption spectrum has been obtained. Irradiation at >640 nm converts this into an isomer which is identical with that formed by ionization of 1,4-dihydro-1,4-ethanonaphtho[1,8-*de*][1,2]diazepine (END) and subsequent irradiation of the radical cation at λ > 540 nm. In both cases, further irradiation at 450 nm yields the radical cation of 1,8-divinylnaphthalene (DVN$^{\bullet+}$) which was identified by ionization of DVN generated *in situ* by photolysis of CAN. These related observations identify the photoisomer of CAN$^{\bullet+}$ as 1,4-perinaphthadiyl radical cation (7,8,9,10-tetrahydrocyclohepta[*de*]naphthalene-7,10-diylium, CND$^{\bullet+}$).

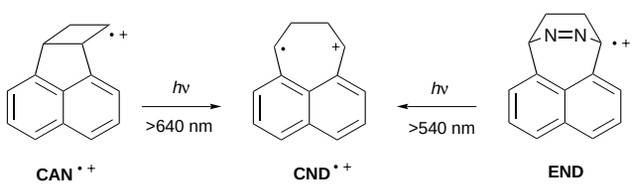

The molecular and electronic structures of all observed radical cations, as well as their electronic absorption spectra, are discussed on the basis of B3LYP and CASPT2 quantum chemical calculations and, in the case of CAN$^{\bullet+}$ and DVN$^{\bullet+}$, also by reference to the photoelectron spectra of the neutral hydrocarbons. The CAN$^{\bullet+}$→PND$^{\bullet+}$→DVN$^{\bullet+}$ sequence of photoreactions is discussed on the basis of orbital and state correlation diagrams.

1 Introduction

The spectroscopic identification and characterization of diradical intermediates involved in hydrocarbon valence isomerization reactions ('no-mechanism reactions') has been a challenge for several decades. Following the pioneering work of Dowd on trimethylene methane,[1,2] 1,8-naphthoquinodimethane diradicals were among the early examples of non-Kekulé π,π-diradicals that were found to be persistent in their triplet ground state at cryogenic temperatures and were thoroughly characterized by various spectroscopic methods.[3–5] The ethylene bridged derivative, 7,8,9,10-tetrahydro**c**yclohepta[*de*]-**n**aphthalene-7,10-**d**iyl (**CND**), which can be conveniently generated from the azo compound, 1,4-dihydro-1,4-**e**thano**n**aphtho[1,8-*de*][1,2]**d**iazepine (**END**), has received special attention as an intermediate in the intramolecular cycloaddition of 1,8-**di**vinyl**n**aphthalene (**DVN**) to form **c**yclobut[*a*]**ac**e**n**aphthylene (**CAN**).[6–8]

Spectroscopic characterization of reactive intermediates opens the way to kinetic studies of their reactivity and the determination of their thermochemical properties. Time-resolved studies of diradicals have provided lifetimes and reactivities of numerous diradical intermediates in solution,[9] including parent 1,8-naphthoquinodimethane.[10] Most of these data pertain to triplet diradicals which are protected from intramolecular stabilization by the spin barrier. Singlet diradicals are usually quite short-lived, *e.g.*, the ring closure of tri- and tetra-methylene occurs on the sub-picosecond timescale.[11–13] Nevertheless, singlet diradicals can be kinetically stabilized by electronic, steric and strain effects, and such systems have been observed by transient optical spectroscopy. Kinetic studies of singlet diradicals include systems in which the radical centers are bridged by a heteroatom,[14] localized cyclopentane-1,3-diyl derivatives,[15,16] and several derivatives of 1,8-naphthoquinodimethane,[17–19] in particular **CND**.[8] These diradicals are protected by a substantial barrier from intramolecular bond formation, so that they are susceptible to diffusional trapping. Several of these studies have also provided thermo-

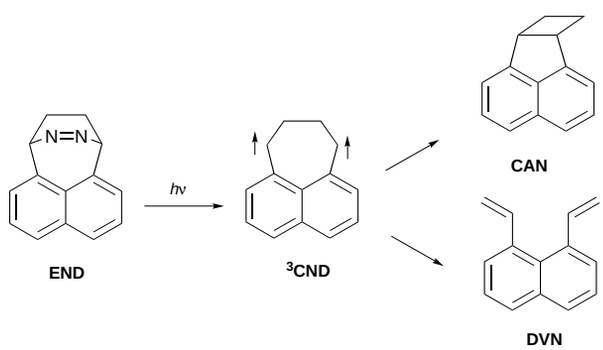

Scheme 1

† Present address: Department of Chemistry, Ohio State University, Columbus, OH 43210, USA.

chemical data, namely activation energies and reaction enthalpies.

The ionization energies of diradicals with essentially non-bonding electrons are expected to be substantially lower than those of related closed shell systems. Hence, radical cations formed by ionization of diradicals will be relatively stable compared with their isomers formed from stable neutral precursors. This is confirmed for example by the finding that, on ionization, hexa-1,5-diene or semibullvalene collapse spontaneously to symmetric radical cations with a structure like that of the diradicaloid transition states for their degenerate Cope rearrangement (Scheme 2), which led Williams to coin the term 'inverted potential energy surface' for such cases.[20]

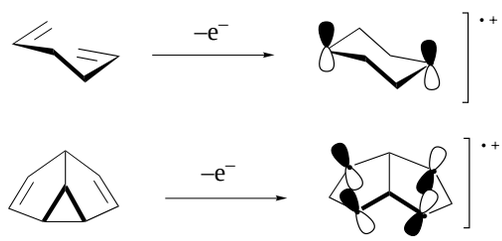

Scheme 2

Other examples of stable diradical ions that were studied in condensed phase include the radical cations of cyclopentane-1,3-diyl[21,22] and trimethylenemethane[23] as well as the radical anion[24] and cation of tetramethylene ethane[25] whose neutral had also been studied by Dowd.[26] More recently, ionized diradicals have been studied extensively in the gas phase. On the one hand, Kenttämaa introduced the use of the ionized forms of phenyl radicals substituted by easily oxidizable nucleophiles (which are also ionized diradicals) to study the chemistry of phenyl radicals in the gas phase,[27] and recently extended this technique even to the study of charged diradicals (=triradical cations).[28] On the other hand, new techniques were developed for the preparation of diradical *anions* in the gas phase which opened the way to the study of the thermochemistry of the corresponding neutral diradicals.[29] Subjecting the same ions to negative photoelectron spectroscopy yields direct information on singlet/triplet gaps, as demonstrated recently for trimethylenemethane[30] and *m*-xylylene.[31]

Our interest in the structures and rearrangements of radical cations[32–34] led us to wonder how the electronic structure and the interconversions of the compounds shown in Scheme 1 would be affected by ionization. In particular, we were attracted by the following questions: (*a*) would the azo compound, **END**, and the cyclobutane derivative, **CAN**, form stable radical cations or decay by spontaneous loss of N_2 or ring opening, respectively, and (*b*) would the radical cation of **CND** be a detectable intermediate and what would be its ground state structure and symmetry? The above questions have a bearing on the possible use of ionized diradicals or their precursors as synthetic intermediates generated by photoinduced electron transfer[35] or chemical oxidation.

2 Experimental

Syntheses

END[8] and **CAN**[6] were samples left from earlier work and were purified by recrystallization before use.

Matrix isolation spectroscopy

Solutions of the precursors [$(1–5) \times 10^{-3}$ M] in a mixture of Freons (equal parts of $CFCl_3$ and CF_2BrCF_2Br)[36,37] or *n*-butyl chloride–isopentane[38,39] were exposed to 0.5 MRad of ^{60}Co γ-irradiation at 77 K. Electronic absorption (EA) spectra were recorded between 190 and 1500 nm with a Perkin-Elmer Lambda 19 instrument.

Photoelectron spectroscopy

Photoelectron (PE) spectra were recorded on a modified Perkin-Elmer PE16 spectrometer operated in preretardation (and hence constant resolution) mode under computer control.[40] Calibration was effected with a Xe–Ar mixture and the spectral resolution was 12 meV (digital resolution 2 meV).

Quantum chemical calculations

The geometries of all species were optimized by the B3LYP density functional method[41–44] as implemented in the GAUSSIAN 94 package of programs,[45] using the 6–31G* basis set. All stationary points were identified by Hessian calculations at the same level (except where otherwise indicated).

Two models were used in calculations of excited states: wherever possible we used the CASSCF/CASPT2 procedure[46] with the MOLCAS program.[47] The active spaces were chosen such that the weight of the CASSCF wavefunction in the final CASPT2 wavefunction was between 60 and 65% for all states considered (a description of the active spaces for each molecule is given in the footnotes to Tables 1–3). As in previous cases of radical cations,[48,49] satisfactory agreement with experiment was obtained with the simple [C]3s2p1d/[H]2s ANO DZ basis set,[50] therefore we saw no necessity to add higher angular momentum and/or diffuse functions.

For **END**$^{\bullet+}$, where CASPT2 calculations were not feasible owing to excessive memory or CPU requirements, we resorted to the semiempirical INDO/S-CI procedure[51] based on ROHF orbitals, whereby only singly excited configurations were taken into account. The INDO/S-CI calculations were performed with the ZINDO program.[52] Molecular orbitals were plotted with the MOPLOT program[53] which gives a schematic representation of the MO's nodal structures in a ZDO-type approximation.[54]

3 Results and discussion

3.1 The radical cation of cyclobut[*a*]acenaphthylene (CAN)

Fig. 1 shows the electronic absorption (EA) spectrum obtained after γ-irradiation of **CAN** in a Freon matrix at 77 K, juxtaposed on a common energy scale to the photoelectron (PE) spectrum and the results of the CASPT2 calculations which are listed numerically in Table 1. Both PE and EA spectra have a similar appearance to those of acenaphthene[49] and they match well with the theoretical predictions and with qualitative expectations.

The first transition ($1^2A''\rightarrow1^2A'$) which is dipole forbidden in the parent naphthalene radical cation still carries too little oscillator strength to allow its detection in **CAN**$^{\bullet+}$, in accord with the fact that the highest two occupied π-MOs of naphthalene are only slightly perturbed by the cyclobutane moiety. As in other naphthalene derivatives, the next transition in the EA spectrum coincides with the third PE band and is therefore attributed to the same excited state ($2^2A'$) which can essentially be described by HOMO-2 (26a′)→HOMO (21a″) electron promotion. It shows a pronounced 1400 cm^{-1} progression that is presumably associated with skeletal vibrations of the naphthyl moiety.

The next two EA bands correspond to mixed states which both involve commensurate contributions from HOMO (21a″)→LUMO (22a″) and HOMO-4 (20a″)→HOMO (21a″) excitations. As in the case of polyene radical cations,[48] the transition to the lower of these states carries a small transition moment, whereas that to the higher-lying positive combination has a larger one (CASSCF appears to overestimate the disparity of the two bands' intensities). The HOMO→LUMO excitation is mostly localized in the naphthyl moiety whereas the 20a″→HOMO excitation involves pronounced charge transfer from the cyclobutyl to the naphthyl part of **CAN**$^{\bullet+}$. This leads to a small off-diagonal matrix element for interaction between the two excited configurations, which is in agreement

Table 1 Excited states of the radical cation of cyclobut[*a*]acenaphthylene ($CAN^{\bullet+}$)

State	PES eV	EAS eV	CASSCF[a] eV	CASPT2 eV	CASPT2 f[c]	Configurations[b]
$1^2A''$	(7.61)[d]	(0)	(0)	(0)	—	81% $(21a'')^1$
$1^2A'$	1.00	—	1.00	1.25	0	79% 27a′→21a″
$2^2A'$	1.87	1.82	2.05	1.90	0.052	71% 26a′→21a″
						5% 27a′→22a″
$2^2A''$	>2.50[e]	2.47	2.98	2.70	7×10^{-6}	35% 20a″→21a″
						35% 21a″→22a″
$3^2A''$	—	3.14	3.46	3.10	0.133	31% 21a″→22a″
						24% 20a″→21a″
						12% 27a′→28a′

[a] Active space: 11 electrons in seven a′ (four occupied, three virtual) and a″ (2 + 2) MOs. [b] In terms of excitations from or into the 21a″ HOMO. [c] Oscillator strength for electronic transition. [d] First ionization potential of CAN, origin of energy scale for excited states. [e] Onset of σ-ionizations.

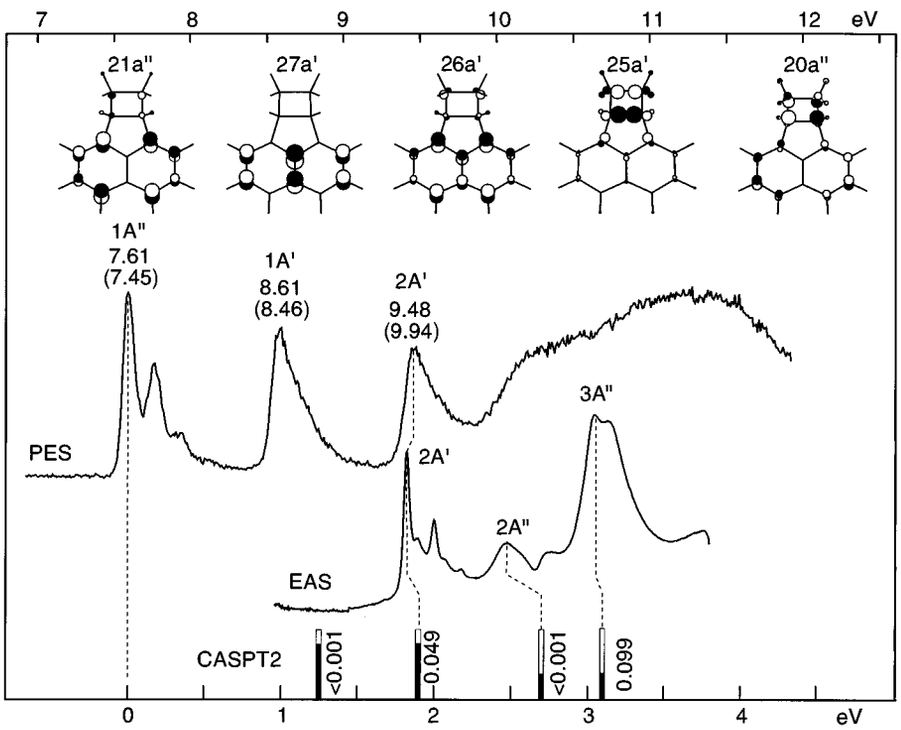

Fig. 1 PE spectrum (upper) of **CAN** and EA spectrum of $\mathbf{CAN}^{\bullet+}$ (lower) drawn on a common energy scale whose origin coincides with the 0–0 transition of the first PE band. Numbers over PE bands denote vertical ionization energies; negative MO energies are given in parentheses. The bars at the bottom represent the results of the CASPT2 calculations listed in Table 1 (the black parts of the bars denote the total weight of Koopmans configurations in final states). MO energies and plots are from RHF/6–31G* calculations.

with the small energy separation of the two final states (0.4 eV). Also, the partial charge transfer from the cyclobutane ring in the course of the excitation into the 2A″ and 3A″ states results in substantial bond length changes, which explains why the second and third bands in the EA spectrum of $\mathbf{CAN}^{\bullet+}$ are not as sharp as in the closely related acenaphthene radical cation.[49]

As with other naphthalene cation derivatives, $\mathbf{CAN}^{\bullet+}$ is expected to have more intense bands in the UV region. However, we did not observe these in the present work because they are hidden by the absorptions of the ionized Freon matrix. Exploratory experiments in argon matrices revealed their presence.

3.2 The radical cation of 1,8-divinylnaphthalene (DVN)

Upon photolysis at 450 nm, the radical cation of **CAN** is transformed cleanly into a new species exhibiting a structured NIR band along with a weak and a strong peak in the visible range. We suspected that this spectrum is due to the radical cation of 1,8-divinylnaphthalene ($\mathbf{DVN}^{\bullet+}$). An authentic sample of **DVN** was not at hand, so we made use of the observation that the azo compound, **END**, can be photodecomposed to yield exclusively **DVN** in organic glasses at 77 K.[8] Exhaustive photolysis of **END** at 400 nm and subsequent γ-irradiation gave a spectrum which was identical with that obtained after the 450 nm irradiation of $\mathbf{CAN}^{\bullet+}$ (yet another way to obtain the same spectrum was by ionizing **END** and photolyzing the resulting radical cation at 450 nm, see below).

The spectrum thus obtained is juxtaposed to the PE spectrum of **DVN**, scanned and replotted from the literature[55] in Fig. 2, which also displays schematically the results of the CASPT2 calculations listed in Table 2. As the HOMO shows a weak antibonding interaction between the naphthyl and the vinyl moieties, it is to be expected that the twisting of the latter, which is due to steric interactions of the α-hydrogen atoms, decreases on ionization. This is confirmed by B3LYP/6-31G* geometry optimizations, which give structures of C_2 symmetry represented in Fig. 3. Indeed, the dihedral angles decrease by 6.4° while the double bond lengths increase by 1.8 pm, geometry changes that have repercussions on the energies of all MOs that involve bonding or antibonding interactions between the naphthyl and the vinyl moieties. This affects in particular the relative position of the first two excited states (1^2B and 2^2B) as is evident from Fig. 2: the second band peaking at 8.73 eV in the PE

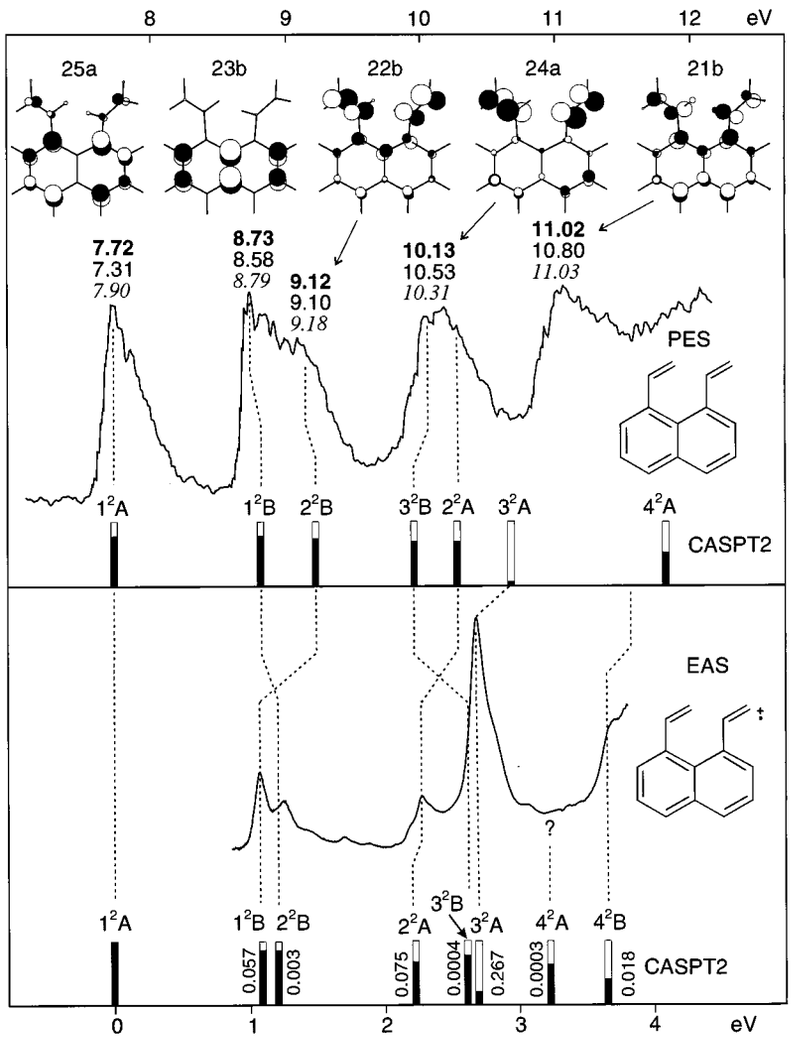

Fig. 2 PE spectrum of **DVN** (upper, scanned from ref. 55) and EA spectrum of **DVN**$^{\bullet+}$ (lower) drawn on a common energy scale whose origin coincides with the 0–0 transition of the first PE band. Bold-face numbers over PE bands denote vertical ionization energies, normal face numbers are ROHF/6–31G*, italic numbers MINDO/3 negative MO energies.[55] The bars at the bottom represent the results from the CASPT2 calculations listed in Table 2 (the black parts of the bars denote the total weight of Koopmans configurations in the final states). MO plots are from RHF/6–31G* calculations.

spectrum of **DVN** had been assigned to ionization from the second occupied π-MO of the naphthalene part,[55] an assignment which is confirmed by our CASPT2 calculations *at the neutral geometry*. However, electron excitation from that MO to the HOMO (which is electric-dipole forbidden in the parent naphthalene radical cation) *at the geometry of the radical cation* is associated with a vanishingly small transition moment. Hence, the rather intense EA band which happens to coincide with the second PE band *cannot* be due to that transition.

Simple MO calculations reveal that the sequence of the second and third highest MO of **DVN** changes on decreasing the twisting angle of the vinyl groups. This is also reflected in the CASPT2 results which show that the observed EA transition is due to electron promotion from the essentially vinylic MO, which in turn gives rise to the shoulder at 9.12 eV in the PE spectrum. The corresponding crossover of states is indicated by dashed lines in Fig. 2. The third PE band, which had originally been assigned on the basis of Koopmans' theorem to ionization from the vinylic MO 24a,[55] is found to 'contain' two states of partial Koopmans character,‡ 3^2B and 2^2A. According to the CASSCF calculations, the first of these corresponds to 51% ionization from MO 21b and 18% ionization from 22b (which contributes 59% to 2^2B), mixed with several non-Koopmans configurations. The 2^2A state is composed to 55% of ionization from MO 24a plus 10% ionization from 23a (not shown in Fig. 2), again mixed with several non-Koopmans configurations, the most important of which corresponds to HOMO→LUMO excitation.§

Turning to the radical cation spectrum, we note that the 1^2A→3^2B transition has a vanishingly small oscillator strength, therefore it is not expected to show up in the spectrum of **DVN**$^{\bullet+}$. In contrast, the position of the 2^2A state at the cation geometry suggests that it is associated with the weak band at 2.2 eV (note that the sequence of these two excited states changes on going from the neutral to the cation geometry!). The strongest peak in the cation spectrum is undoubtedly due to excitation into the 3^2A state which does not manifest

‡ By Koopmans character we denote the percent weight of excited configurations that do *not* involve virtual MOs and hence contribute intensity to the PE spectrum (states which involve *only* excitations into virtual MOs do not give rise to PE bands).

§ Note that the weight of the Koopmans configurations may be overestimated by the present CASPT2 calculations because the active space (which permitted a satisfactory description of the excited states of interest) contains nine occupied and only four virtual MOs. This imbalance results in the excitations into virtual MOs being underrepresented, especially in higher excited states such as 3^2B and 2^2A. Hence the prediction of two states in the region of the third PE band is not incompatible with its intensity. Owing to limitations in the (17,13) active space we were also unable to assign the fourth PE band which comprises ionizations from lower-lying occupied MOs.

Table 2 Excited states of the radical cation of 1,8-divinylnaphthalene ($DVN^{\bullet+}$)

	Neutral equilibrium geometry					Radical cation equilibrium geometry				
		CASPT2					CASPT2			
State	PES eV	eV	%K[d]	CASSCF[a] eV	CASSCF Configurations[c]	EAS eV	eV	f[e]	CASSCF[b] eV	Configurations[c]
1^2A	(7.72)[f]	(0)	77	(0)	77.4% ground config.	(0)	(0)	—	(0)	81% ground config.
1^2B	1.0	1.08	77	0.78	77.5% 23b→25a	1.16 (m)	1.14	6.0×10^{-2}	1.76	62% 23b→25a 13% 22b→25a 10% 21b→25a
2^2B	1.4	1.49	73	1.53	59.0% 22b→25a 14.2% 21b→25a	?	1.27	1.9×10^{-4}	1.48	71% 22b→25a 12% 23b→25a
3^2B	2.4	2.23	68	2.97	50.9% 21b→25a 17.7% 22b→25a	?	2.61	1.4×10^{-4}	3.62	70% 21b→25a 8% 23b→25a
2^2A	2.4	2.55	65	2.76	54.5% 24a→25a 10.1% 23a→25a *4.3% 25a→26a*	2.34 (m)	2.23	7.5×10^{-2}	3.06	48% 24a→25a 18% 23a→25a *14% 25a→26a*
3^2A	3.3	2.98	6	3.33	*41.1% 25a→26a* *9.9% 24a→27a* *6.6% 24a→26a*	2.74 (s)	2.69	2.7×10^{-1}	3.58	*57% 25a→26a* 20% 24a→25a
4^2A	3.3	(4.09)	59	3.80	47.4% 23a→25a 11.6% 22a→25a *6.1% 23b→24b*	?	3.22	3.2×10^{-4}	4.20	46% 23a→25a 17% 24a→25a *10% 23b→24b*
4^2B	?	(4.89)	36	4.53	35.6% 20b→25a + *other configs.*	>3.6 (m)	3.65	2.2×10^{-2}	4.56	34% 20b→25a *20% 25a→26b* *11% 22b→26a*

[a] Active space: 17 electrons in four occupied/two virtual MOs of a-symmetry and five occupied/two virtual MOs of b-symmetry. [b] Active space for A-states: 15 electrons in five occupied/three virtual MOs of a-symmetry and two occupied/two virtual MOs of b-symmetry; active space for B-states: 15 electrons in three occupied/one virtual MOs of a-symmetry and five occupied/three virtual MOs of b-symmetry. [c] In terms of single excitations into or from the 25a SOMO. [d] Percent Koopmans character, proportional to intensity of the PE band. [e] Oscillator strength for electronic transition, computed on the basis of the CASSCF wavefunction, using the CASPT2 energy difference in the denominator. [f] First ionization potential of DVN, origin of energy scale for excited states.

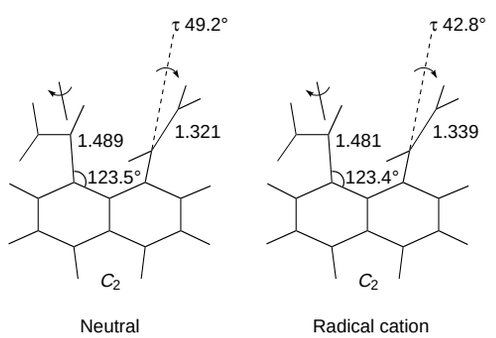

Fig. 3 Geometries of **DVN** and $\mathbf{DVN}^{\bullet+}$ from B3LYP/6-31G* calculations (only the most important parameters are shown)

itself in the PE spectrum due to its high non-Koopmans character (57% HOMO→LUMO promotion). At 3.7 eV we can discern the onset of another EA band, but the present calculations did not permit a definitive assignment.¶

3.3 Photochemistry of $\mathbf{CAN}^{\bullet+}$ and $\mathbf{END}^{\bullet+}$: the 1,4-perinaphthadiyl radical cation

As mentioned above, irradiation of the cyclobutane derivative, $\mathbf{CAN}^{\bullet+}$, or the diazo cation, $\mathbf{END}^{\bullet+}$, at 450 nm leads to the radical cation of 1,8-divinylnaphthalene, $\mathbf{DVN}^{\bullet+}$. However, we suspected that the primary product of both photoreactions may be the 1,4-perinaphthadiyl radical cation, 7,8,9,10-tetrahydrocyclohepta[*de*]naphthalene-7,10-diylium ($\mathbf{CND}^{\bullet+}$) which arises by loss of N_2 from $\mathbf{END}^{\bullet+}$ or by cleavage of one of the cyclobutane bonds of $\mathbf{CAN}^{\bullet+}$. In order to probe this possibility, we carried out photolyses at longer wavelengths to avoid possible secondary photodegradation of the presumed intermediate.

Figs. 4 and 5 show the results of these efforts: irradiation of $\mathbf{CAN}^{\bullet+}$ or $\mathbf{END}^{\bullet+}$ through a 640 nm cutoff filter leads in both cases to the same spectrum (*b*) of a persistent intermediate, which can readily be transformed into $\mathbf{DVN}^{\bullet+}$ (*c*) by ensuing 450 nm photolysis. Before discussing the assignment of this intermediate spectrum we wish to comment briefly on that of $\mathbf{END}^{\bullet+}$ [Fig. 5(*a*)], in particular the conspicuous broad NIR band peaking at 10 000 cm^{-1}. INDO/S does predict a transition in this region (*cf.* $1^2A'$ in Fig. 5), but this corresponds essentially to the HOMO-1→HOMO excitation of $\mathbf{CAN}^{\bullet+}$, which is associated with a very weak oscillator strength and hence cannot be responsible for the observed strong NIR band.

The next transition, which carries an oscillator strength that is more commensurate with the observed band intensity, is predicted to be 0.6 eV higher in energy, *i.e.*, in the visible region. It is associated with excitation from the n_N-MO to the HOMO, *i.e.* with substantial charge transfer from the azo to the naphthyl moiety. Part of the reason why this transition is predicted to be 0.68 eV too high is that the n_N-MOs generally lie too low in energy according to INDO/S; whereas in $\mathbf{END}^{\bullet+}$ the energy difference between the n_N (HOMO-4) and the HOMO is 2.3 eV by INDO/S, it is only 1.8 eV by RHF/3–21G. Higher excited states of $\mathbf{END}^{\bullet+}$ appear to be predicted in better accord with experiment, as shown by the bars in Fig. 5, but we hesitate to propose a definitive assignment of the entire spectrum of $\mathbf{END}^{\bullet+}$ on the basis of these calculations.

¶ In the CASPT2 calculations at the radical cation geometry, we found it impossible to arrive at a satisfactory description of all states of interest with the same active space that had been used to model the PE spectrum. Thus, we resorted to the choice of active orbitals and electrons described in footnote *b* of Table 2 which allowed us to obtain CASPT2 wavefunctions for the first four states of A and B symmetry without perturbations from intruder states.

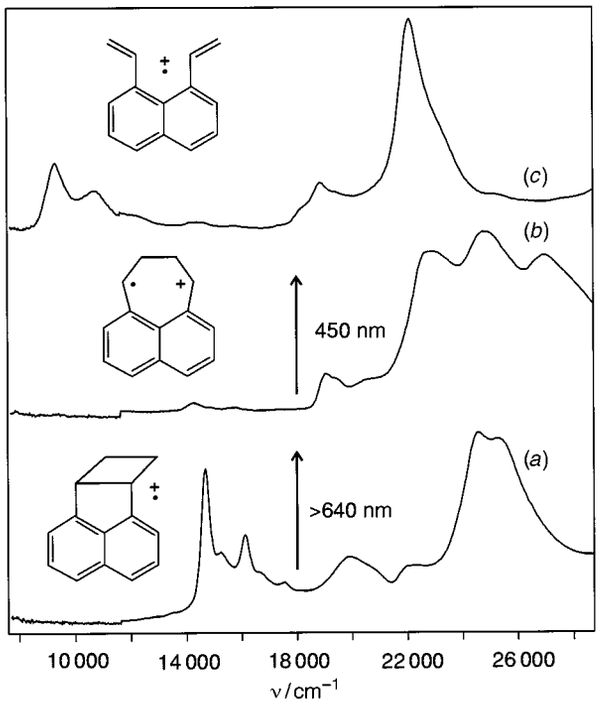

Fig. 4 Stepwise phototransformation of **CAN**$^{\bullet+}$ (*a*) *via* **CND**$^{\bullet+}$ (*b*) into **DVN**$^{\bullet+}$ (*c*)

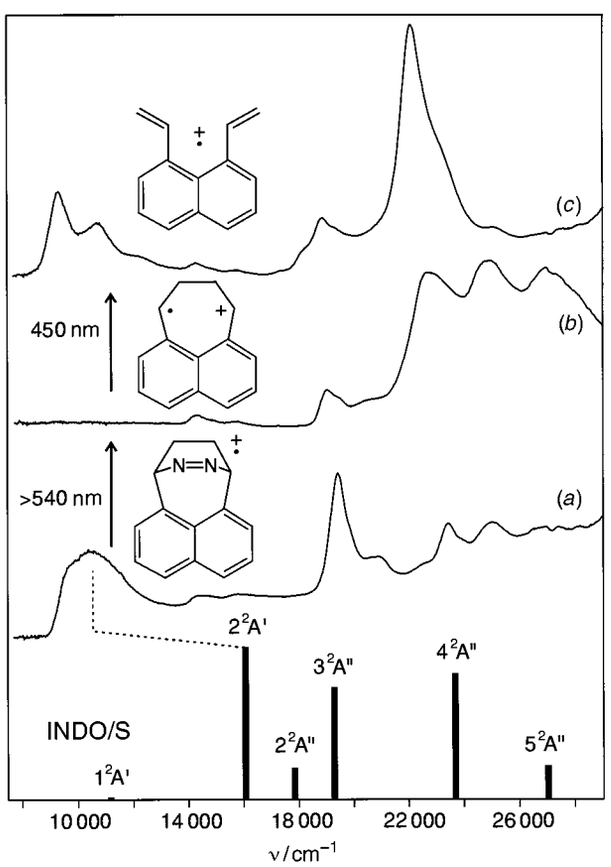

Fig. 5 Stepwise phototransformation of **END**$^{\bullet+}$ (*a*) *via* **CND**$^{\bullet+}$ (*b*) into **DVN**$^{\bullet+}$ (*c*). The bars at the bottom are INDO/S predictions for electronic transitions of **END**$^{\bullet+}$ (height is proportional to oscillator strength). For a discussion see the text.

Returning to the intermediate spectrum depicted in traces (*b*) of Figs. 4 and 5, we note the absence of any significant absorptions above 530 nm, whereas there are several intense bands in the near UV region. In an effort to understand the electronic structure of the presumed intermediate, **CND**$^{\bullet+}$, we undertook

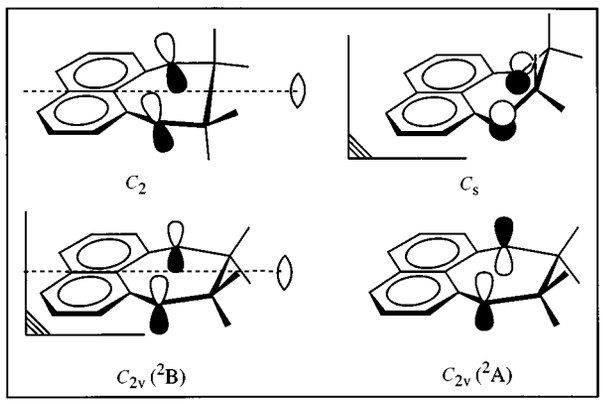

Fig. 6 Schematic representation of 'bent' (C_s) and 'twist' (C_2) conformations of **CND** and of the symmetric and antisymmetric MOs in C_{2v} symmetry

quantum chemical calculations, which are described and discussed below.

Neutral **CND** has a triplet ground state,[7] which implies that the two singly occupied MOs are very close in energy. If such a species is ionized, two states of different symmetry but similar energy can be formed, depending on which of the two nearly degenerate MOs is vacated. Therefore, any discussion of ionized diradicals must involve consideration of two possible ground states corresponding to single occupation of one or the other non-bonding MO. In the present case, the two MOs are derived from the NBMOs of the 1,8-naphthoquinodimethane system whose main components are the positive and negative combinations of the terminal p-AOs in the butane-1,4-diyl bridge (*cf.* Fig. 6).

In the case of **CND** an additional complication arises because of the conformational flexibility of this bridge. Watson *et al.* had already proposed that a planar C_{2v} equilibrium conformation of **CND** was unlikely due to angular strain in the seven-membered ring.[6] Instead they examined two conformers which they called 'twist' (C_2) and 'bent' (C_s, see Fig. 6) and concluded from experiments on deuteriated derivatives that the two must be in rapid equilibrium. They also noted that the bent conformation was well disposed to either cleavage to give **DVN** or collapse to **CAN**.

Geometry optimizations at the B3LYP or ROHF/6–31G* level revealed that the planar C_{2v} structure is a transition state for interconversion of two 'twist' C_2 minima in both possible ground states of **CND**$^{\bullet+}$ ($^2A_2$ and $^2B_1$ in C_{2v}).‖ All attempts to locate a 'bent' minimum by geometry optimization within C_s symmetry resulted either in collapse to C_{2v} **CND**$^{\bullet+}$ or (when starting with strongly bent geometries) to **CAN**$^{\bullet+}$. Thus, there appears to be only one equilibrium conformation of **CND**$^{\bullet+}$ and it corresponds to the 'twist' structure proposed by Watson *et al.* The activation barrier for interconversion of two such structures *via* a C_{2v} transition state as well as the energy separation between the ^{2}A and the ^{2}B state depend slightly on the theoretical model used (see Fig. 7), but those that we employed (B3LYP, ROHF, ROMP2) all agree, predicting that ^{2}B is the ground state.

CASPT2 excited state calculations based on the above premise resulted in the predictions represented graphically at the bottom of Fig. 8 and listed in Table 3. Of course the first excited state at 0.5 eV is the ^{2}A state, which is associated with promotion of the single electron from the lower- to the higher-

‖ The frequency analyses were carried out on structures optimized with the 3-21G basis set. As the energy differences between the two stationary points were found to depend little on the basis set, we assume that the analysis that results from the frequency calculations with the smaller basis set can be carried over to the results obtained with the 6-31G* basis.

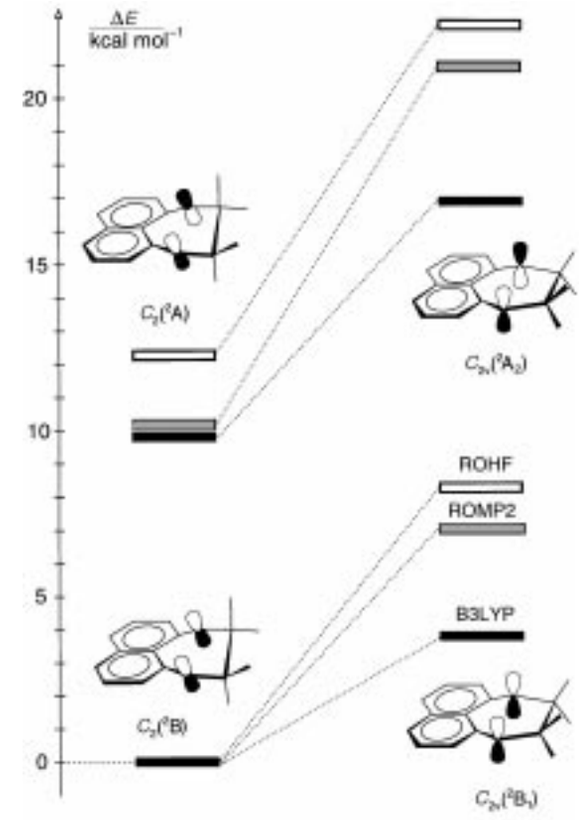

Fig. 7 Relative energy of C_2 ('twist') and C_{2v} conformations and of $^2A_{(2)}$ and $^2B_{(1)}$ states of **CND**$^{\bullet+}$, by B3LYP (black bars), ROHF (white bars) and ROMP2 (gray bars). The C_{2v}/C_2 energy difference denotes the activation barrier for interconversion of two C_2 conformations.

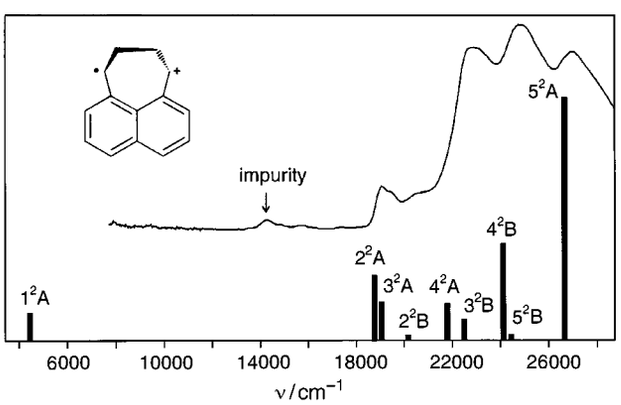

Fig. 8 Spectrum attributed to **CND**$^{\bullet+}$ and graphical representation of the CASPT2 predictions for this species listed in Table 3

energy non-bonding MO. After a gap of nearly 2 eV a tightly spaced group of transitions spreads over about 1 eV, many of which carry oscillator strengths that indicate detectable bands of various intensity.

Analysis of the composition of the CASSCF wavefunctions (*cf*. last column of Table 3) indicates extensive configurational mixing in all of the higher excited states, therefore we refrain from presenting a detailed analysis of the electronic structure of **CND**$^{\bullet+}$. Also, we cannot propose detailed assignments of the different bands in the spectrum, but if we assume that the accuracy of the CASPT2 does not deviate from the usual ±0.2 eV, then the predicted spectrum is in qualitative accord with the observed one. This constitutes no structural proof, but we can think of no alternative intermediate in the photochemical conversions depicted in Figs. 5 and 6 which could give rise to the observed spectrum.

An additional experimental observation serves to support

Table 3 Excited states of the radical cation of 7,8,9,10-tetrahydrocyclohepta[*de*]naphthalene-7,10-diylium (CND$^{\bullet+}$)

State	EAS eV	CASSCF[a] eV	CASPT2 eV	CASPT2 *f*[c]	Major configurations[b]
1^2B	(0)	(0)	(0)	—	72% (23b)^1
1^2A	—	0.48	0.51	0.019	68% 23b→26a
2^2A	2.35	2.53	2.36	0.041	21% 23b→26a+ 25a→26a 14% 23b→28a 9% 23b→27a
3^2A	2.55	3.10	2.32	0.023	24% 25a→23b 16% 22b→26a 9% 23b→27a 8% 21b→26a
2^2B	—	2.66	2.53	0.002	30% 22b→23b 26% 23b→26a+ 25a→26a
4^2A	2.8	2.94	2.70	0.023	37% 22b→26a 12% 25a→23b 5% 21b→26a
3^2B	2.8	3.28	2.81	0.013	23% 23b→24b 10% 21b→23b 10% 25a→26a
4^2B	3.0	3.39	2.98	0.062	30% 25a→26a 12% 23b→24b 8% 23b→26a+ 21b→26a
5^2B	3.0	3.64	3.05	0.003	21% 25a→26a 11% 23b→24b 9% 21b→23b
5^2A	3.3	3.93	3.28	0.147	38% 22b→26a 6% 22b→27a

[a] Active space: 11 electrons in five MOs of a-symmetry (two occupied, three virtual) and seven of b-symmetry (four occupied, three virtual) MOs. [b] From CASSCF wavefunction. [c] Oscillator strength for electronic transition.

our assignment: following the procedure described by Gisin *et al*.[7] we exposed a sample of the azo precursor, **END**, in a mixture of butyl chloride and isopentane to monochromatic 405 nm irradiation which converted it into a mixture of the diradical, **CND** (clearly discernible by its sharp absorptions around 500 nm and the strong peaks at <340 nm), and some **DVN**. Ionization of that sample resulted in a spectrum which shows the features of the intermediate observed in the photo-transformations of **CAN**$^{\bullet+}$ or **END**$^{\bullet+}$, albeit not as well resolved (see Fig. 9). Irradiation of that sample at 450 nm converted the spectrum cleanly into that of **DVN**$^{\bullet+}$. Thus, ionization of pre-formed **CND** seems to yield the intermediate seen in the experiments, which supports our assignment of this species to **CND**$^{\bullet+}$.

Finally we present an orbital correlation scheme (Fig. 10) which demonstrates that both steps in the **CAN**$^{\bullet+}$→ **CND**$^{\bullet+}$→ **DVN**$^{\bullet+}$ reaction sequence observed in our experiments involve state crossings, *i.e*. the ground states of the reactants correlate with excited states of the products. This, together with the fact that according to B3LYP/6-31G* both steps are endothermic, explains why none of these reactions occurs spontaneously, but require population of excited states by irradiation.

4 Conclusions

Scheme 3 summarizes the observations reported in this work. We have shown that cyclobut[*a*]acenaphthylene (**CAN**) forms a

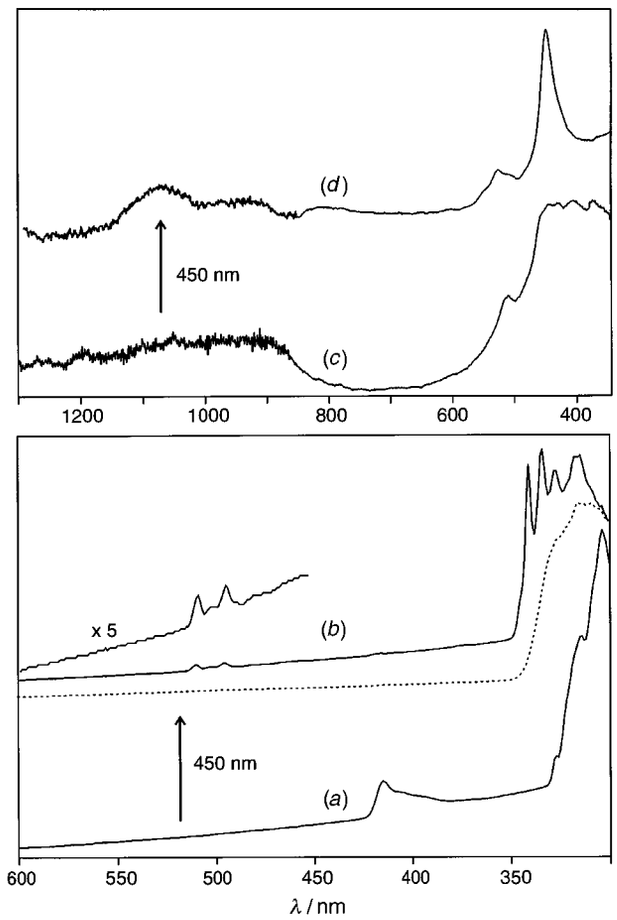

Fig. 9 Phototransformation of END (*a*) into a mixture of **CND** and **DVN** (*b*, the dashed line shows the spectrum of pure **DVN**) and results of subsequent ionization (*c*) and 450 nm photolysis to yield $\mathbf{DVN}^{\bullet+}$ (*d*)

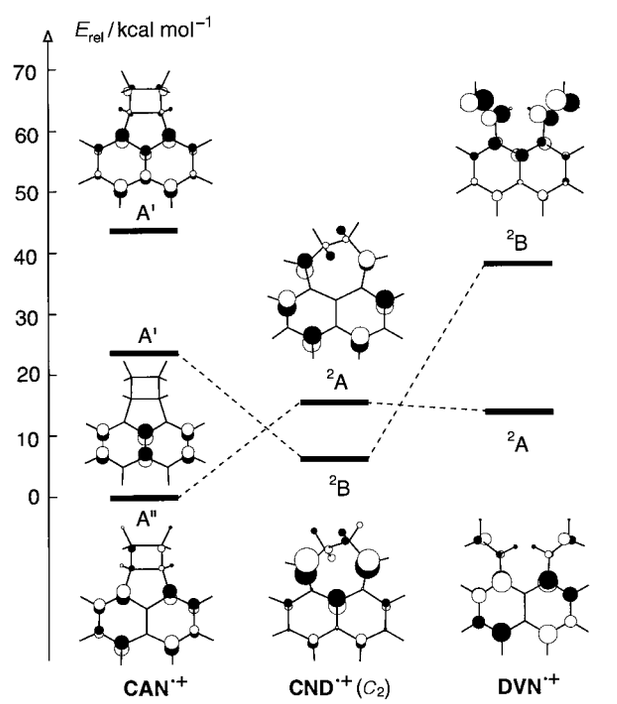

Fig. 10 State correlation diagram for the $\mathbf{CAN}^{\bullet+} \rightarrow \mathbf{CND}^{\bullet+} \rightarrow \mathbf{DVN}^{\bullet+}$ reaction. MO plots represent the singly occupied MO in each state (from ROHF/6-31G* calculations).

stable radical cation on ionization which can be transformed in two distinct photochemical steps into that of 1,8-divinylnaphthalene (**DVN**). The intermediate which occurs in that

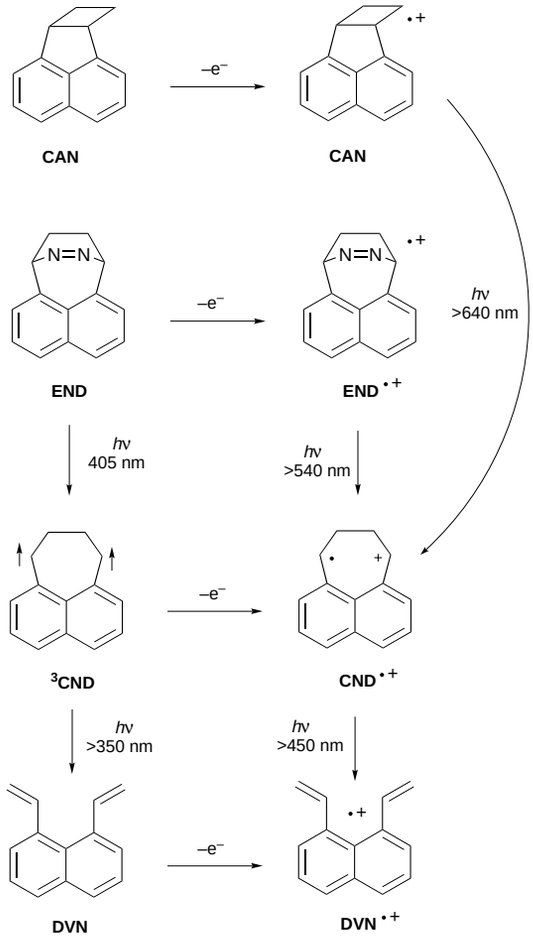

Scheme 3 Summary of results of the present study

reaction can be formed independently from the azo precursor, **END**, either by irradiation to yield the 1,4-perinaphthadiyl diradical, **CND**, and subsequent ionization, or by photodeazotation of ionized **END** at >640 nm. Irradiation at 450 nm irreversibly converts this intermediate into $\mathbf{DVN}^{\bullet+}$. From the above experiments, as well as from the quantum chemical calculations described in Section 3.3, we conclude that this intermediate corresponds to the ionized diradical, $\mathbf{CND}^{\bullet+}$. To the best of our knowledge this represents the first observation of an ionized diradical by optical spectroscopy.

Acknowledgements

This work was been funded through grant No. 2028–047212.96 of the Swiss National Science Foundation.

References

1 P. Dowd, *J. Am. Chem. Soc.*, 1966, **88**, 2587.
2 P. Dowd and M. Chow, *Tetrahedron*, 1982, **38**, 799.
3 M. Rule, A. R. Matlin, D. E. Seeger, E. F. Hilinski, D. A. Dougherty and J. A. Berson, *Tetrahedron*, 1982, **38**, 787.
4 M. S. Platz, in *Diradicals*, ed. W. T. Borden, Wiley, New York, 1982.
5 J. Wirz, *Pure Appl. Chem.*, 1984, **56**, 1289.
6 C. R. Watson, R. M. Pagni, J. R. Dodd and J. E. Bloor, *J. Am. Chem. Soc.*, 1976, **98**, 2551.
7 M. Gisin, E. Rommel, J. Wirz, M. N. Burnett and R. M. Pagni, *J. Am. Chem. Soc.*, 1979, **101**, 2216.
8 M. N. Burnett, R. Boothe, E. Clark, M. Gisin, H. M. Hassaneen, R. M. Pagni, G. Persy, R. J. Smith and J. Wirz, *J. Am. Chem. Soc.*, 1988, **110**, 2527.
9 L. J. Johnston and J. C. Scaiano, *Chem. Rev.*, 1989, **89**, 521.
10 M. C. Biewer, M. S. Platz, M. Roth and J. Wirz, *J. Am. Chem. Soc.*, 1991, **113**, 8069.
11 S. Pedersen, J. L. Herek and A. H. Zewail, *Science*, 1994, **266**, 1293.
12 A. H. Zewail, *J. Phys. Chem.*, 1996, **100**, 12 701.

13 C. Doubleday, K. Bolton and W. L. Hase, *J. Am. Chem. Soc.*, 1997, **119**, 5251.
14 J. A. Berson, *Acc. Chem. Res.*, 1997, **30**, 238.
15 W. Adam, W. T. Borden, C. Burda, H. Foster, T. Heidenfelder, M. Heubes, D. A. Hrovat, F. Kita, S. B. Lewis, D. Scheutzow and J. Wirz, *J. Am. Chem. Soc.*, 1998, **120**, 593.
16 W. Adam, H. Platsch and J. Wirz, *J. Am. Chem. Soc.*, 1989, **111**, 6896.
17 E. Hasler, A. Hörmann, G. Persy, H. Platsch and M. Wirz, *J. Am. Chem. Soc.*, 1993, **115**, 5400.
18 D. R. McMasters, J. Wirz and G. J. Snyder, *J. Am. Chem. Soc.*, 1997, **119**, 8568.
19 W. R. Roth, C. U. Unger and T. Wasser, *Liebigs Ann. Chem.*, 1996, **12**, 2155.
20 F. Williams, *J. Chem. Soc.*, *Faraday Trans.*, 1994, **90**, 1681.
21 F. Williams, Q.-X. Guo, T. M. Kolb and S. F. Nelsen, *J. Chem. Soc.*, *Chem. Commun.*, 1989, 1835.
22 W. Adam, C. Sahin, J. Sendelbach, H. Walter, G.-F. Chen and F. Williams, *J. Am. Chem. Soc.*, 1994, **116**, 2576.
23 K. Komaguchi, M. Shiotani and A. Lund, *Chem. Phys. Lett.*, 1997, **265**, 217.
24 N. L. Bauld and G. R. Stevenson, *J. Am. Chem. Soc.*, 1969, **91**, 3675.
25 F. Gerson, A. de Meijere and X.-Z. Qin, *J. Am. Chem. Soc.*, 1989, **111**, 1135.
26 (*a*) P. Dowd, *J. Am. Chem. Soc.*, 1970, **92**, 1066; (*b*) P. Dowd, W. Chang and Y. H. Paik, *J. Am. Chem. Soc.*, 1986, **108**, 7416.
27 R. L. Smith and H. Kenttämaa, *J. Am. Chem. Soc.*, 1995, **117**, 1393.
28 K. N. Thoen and H. I. Kenttämaa, *J. Am. Chem. Soc.*, 1997, **119**, 3832.
29 See, for example: P. G. Wenthold, J. Hu and R. R. Squires, *J. Am. Chem. Soc.*, 1996, **118**, 11 865.
30 P. G. Wenthold, J. Hu, R. R. Squires and W. C. Lineberger, *J. Am. Chem. Soc.*, 1996, **118**, 475.
31 P. G. Wenthold, J. B. Kim and W. C. Lineberger, *J. Am. Chem. Soc.*, 1997, **119**, 1354.
32 T. Bally, in *Radical Ionic Systems* (*Top. Mol. Organization Eng.*, Vol. 6), ed. A. Lund and M. Shiotani, Kluwer, Dordrecht, 1991, pp. 3–54.
33 T. Bally, *Chimia*, 1994, **48**, 378.
34 T. Bally, L. Truttmann, J. T. Wang and F. Williams, *J. Am. Chem. Soc.*, 1995, **117**, 7923.
35 H. Weng, C. Scarlata and H. D. Roth, *J. Am. Chem. Soc.*, 1996, **118**, 10 947.
36 C. Sandorfy, *Can. J. Spectrosc.*, 1965, **85**, 10.
37 A. Grimison and G. A. Simpson, *J. Phys. Chem.*, 1968, **72**, 1776.
38 T. Shida and W. H. Hamill, *J. Am. Chem. Soc.*, 1966, **88**, 5371.
39 T. Shida and W. H. Hamill, *J. Chem. Phys.*, 1968, **44**, 4372.
40 R. Dressler, L. Neuhaus and M. Allan, *J. Electron Spectr. Relat. Phenom.*, 1983, **31**, 181.
41 A. D. Becke, *Phys. Rev. A*, 1988, **39**, 3098.
42 A. D. Becke, *J. Chem. Phys.*, 1993, **98**, 5648.
43 C. Lee, W. Yang and R. G. Parr, *Phys. Rev. B*, 1988, **37**, 785.
44 For a description of the density functionals implemented into the GAUSSIAN program 45, see: B. G. Johnson, P. M. W. Gill and J. A. Pople, *J. Chem. Phys.*, 1993, **98**, 5612.
45 M. J. Frisch, G. W. Trucks, H. B. Schlegel, P. M. W. Gill, B. G. Johnson, M. A. Robb, J. R. Cheeseman, T. Keith, G. A. Petersson, J. A. Montogomery, K. Raghavachari, M. A. Al-Laham, V. G. Zakrzewski, J. V. Ortiz, J. B. Foresman, J. Cioslowski, B. B. Stefanov, A. Nanayakkara, M. Challacombe, C. Y. Peng, P. Y. Ayala, W. Chen, M. W. Wong, J. L. Andres, E. S. Repogle, R. Gomperts, R. L. Martin, D. J. Fox, J. S. Binkley, D. J. DeFrees, J. Baker, J. P. Stewart, M. Head-Gordon, M. C. Gonzales and J. A. Pople. GAUSSIAN Program; GAUSSIAN 94, Rev. B1 and D4; Gaussian, Inc., Pittsburgh, PA, 1995.
46 K. Andersson and B. O. Roos in *Modern Electronic Structure Theory*, Part 1, Vol. 2, World Scientific., Singapore, 1995, pp. 55.
47 K. Andersson, M. R. A. Blomberg, M. P. Fülscher, V. Kellö, R. Lindh, P.-Å. Malmqvist, J. Noga, J. Olson, B. O. Roos, A. Sadlej, P. E. M. Siegbahn, M. Urban and P.-O. Widmark. MOLCAS 3, University of Lund, Sweden, 1994.
48 M. P. Fülscher, S. Matzinger and T. Bally, *Chem. Phys. Lett.*, 1995, **236**, 167.
49 T. Bally, C. Carra, Z. Zhu and M. Fülscher, unpublished results.
50 P.-O. Widmark, P.-Å. Malmqvist and B. O. Roos, *Theor. Chim. Acta*, 1990, **77**, 291.
51 M. C. Zerner and J. E. Ridley, *Theor. Chim. Acta*, 1973, **32**, 111.
52 M. C. Zerner. ZINDO; Quantum Theory Project, University of Florida, Gainesville.
53 T. Bally, B. Albrecht, S. Matzinger and M. G. Sastry. MOPLOT, a program for displaying results of LCAO-MO calculations, available from Thomas.Bally@unifr.ch on request, University of Fribourg, 1997.
54 E. Haselbach and A. Schmelzer, *Helv. Chim. Acta*, 1979, **54**, 1299.
55 R. Gleiter, W. Schaefer and M. Eckert-Maksic, *Chem. Ber.*, 1981, **114**, 2309.

Paper 7/07284H
Received 8*th October* 1997
Accepted 23*rd December* 1997